

# 1 Structurally divergent and recurrently mutated regions of 2 primate genomes

3  
4 Yafei Mao<sup>1,2</sup>, William T. Harvey<sup>1</sup>, David Porubsky<sup>1</sup>, Katherine M. Munson<sup>1</sup>, Kendra  
5 Hoekzema<sup>1</sup>, Alexandra P. Lewis<sup>1</sup>, Peter A. Audano<sup>1</sup>, Allison Rozanski<sup>1</sup>, Xiangyu Yang<sup>2</sup>,  
6 Shilong Zhang<sup>2</sup>, David S. Gordon<sup>1,3</sup>, Xiaoxi Wei<sup>2</sup>, Glennis A. Logsdon<sup>1</sup>, Marina Haukness<sup>4</sup>,  
7 Philip C. Dishuck<sup>1</sup>, Hyeonsoo Jeong<sup>1</sup>, Ricardo del Rosario<sup>5,6</sup>, Vanessa L. Bauer<sup>7</sup>, Will T.  
8 Fattor<sup>7</sup>, Gregory K. Wilkerson<sup>8,9</sup>, Qing Lu<sup>2</sup>, Benedict Paten<sup>4</sup>, Guoping Feng<sup>5,6</sup>, Sara L.  
9 Sawyer<sup>7</sup>, Wesley C. Warren<sup>10-12</sup>, Lucia Carbone<sup>13-16</sup>, Evan E. Eichler<sup>1,3</sup>

10  
11 1. Department of Genome Sciences, University of Washington School of Medicine, Seattle,  
12 WA, USA

13 2. Bio-X Institutes, Key Laboratory for the Genetics of Developmental and Neuropsychiatric  
14 Disorders, Ministry of Education, Shanghai Jiao Tong University, Shanghai, China

15 3. Howard Hughes Medical Institute, University of Washington, Seattle, WA, USA

16 4. UC Santa Cruz Genomics Institute, University of California, Santa Cruz, Santa Cruz, CA,  
17 USA

18 5. McGovern Institute for Brain Research, Department of Brain and Cognitive Sciences,  
19 Massachusetts Institute of Technology, Cambridge, MA, USA

20 6. Stanley Center for Psychiatric Research, Broad Institute of MIT and Harvard, Cambridge,  
21 MA, USA

22 7. BioFrontiers Institute, Department of Molecular, Cellular, and Developmental Biology,  
23 University of Colorado, Boulder, CO, USA

24 8. Department of Veterinary Sciences, Michale E. Keeling Center for Comparative Medicine  
25 and Research, The University of Texas MD Anderson Cancer Center, Bastrop, TX, USA

26 9. Department of Clinical Sciences, North Carolina State University, Raleigh, NC, USA

27 10. Department of Animal Sciences, Bond Life Sciences Center, University of Missouri,  
28 Columbia, MO, USA

29 11. Department of Surgery, School of Medicine, University of Missouri, Columbia, MO,  
30 USA

31 12. Institute of Data Science and Informatics, University of Missouri, Columbia, MO, USA

32 13. Department of Medicine, Knight Cardiovascular Institute, Oregon Health and Science  
33 University, Portland, OR, USA

34 14. Division of Genetics, Oregon National Primate Research Center, Beaverton, OR, USA

35 15. Department of Molecular and Medical Genetics, Oregon Health and Science University,  
36 Portland, OR, USA

37 16. Department of Medical Informatics and Clinical Epidemiology, Oregon Health and  
38 Science University, Portland, OR, USA

39

40 **ABSTRACT**

41 To better understand the pattern of primate genome structural variation, we sequenced and  
42 assembled using multiple long-read sequencing technologies the genomes of eight nonhuman  
43 primate species, including New World monkeys (owl monkey and marmoset), Old World  
44 monkey (macaque), Asian apes (orangutan and gibbon), and African ape lineages (gorilla,  
45 bonobo, and chimpanzee). Compared to the human genome, we identified 1,338,997 lineage-  
46 specific fixed structural variants (SVs) disrupting 1,561 protein-coding genes and 136,932  
47 regulatory elements, including the most complete set of human-specific fixed differences.  
48 Across 50 million years of primate evolution, we estimate that 819.47 Mbp or ~27% of the  
49 genome has been affected by SVs based on analysis of these primate lineages. We identify  
50 1,607 structurally divergent regions (SDRs) wherein recurrent structural variation contributes  
51 to creating SV hotspots where genes are recurrently lost (*CARDs*, *ABCD7*, *OLAH*) and new  
52 lineage-specific genes are generated (e.g., *CKAP2*, *NEK5*) and have become targets of rapid  
53 chromosomal diversification and positive selection (e.g., *RGPDs*). High-fidelity long-read  
54 sequencing has made these dynamic regions of the genome accessible for sequence-level  
55 analyses within and between primate species for the first time.

56

57 **INTRODUCTION**

58 An early and still unmet grand challenge of the Human Genome Project has been to  
59 reconstruct the evolutionary history of every base pair of the human reference sequence<sup>1-5</sup>.  
60 To do so requires both a diverse sampling of nonhuman primate (NHP) genomes but also a  
61 more complete assembly of those genomes so that all forms of variation can be assessed  
62 without bias introduced from a superior quality reference<sup>6-13</sup>. Early attempts to sequence  
63 closely related ape species focused primarily on characterizing simpler forms of variation  
64 (e.g., single-nucleotide variants, (SNVs)) from portions of the genome that could be readily  
65 aligned to human<sup>7-10,13</sup>. As long-read sequence assemblies began to emerge, our ability to  
66 catalog larger forms of structural variation significantly improved resulting in a series of  
67 more contiguous NHP genomes. These new references, however, represented “squashed”  
68 assemblies where allelic variation was collapsed and the most complex forms of gene-rich  
69 structural variants (SVs) were still not resolved, including recently duplicated sequence<sup>14-19</sup>.  
70 Advances in long-read sequencing technology over the last three years now allow for most of  
71 these regions to be accurately sequenced and assembled to a degree where both paralogous  
72 and allelic variation can be readily distinguished<sup>20-23</sup>. Numerous studies focused on the  
73 human lineage have shown that such regions are incubators for the emergence of new genes,  
74 adaptive evolution while also contributing to disease, and disease susceptibility<sup>24-26</sup>.

75

76 To better characterize SVs and these complex genic SV regions, we generated genome  
77 assemblies of eight NHP genomes using two long-read sequencing platforms. Our plan was  
78 twofold: First, we wanted to broaden the phylogenetic diversity by sequencing additional  
79 NHP genomes using the same sequencing platform (in this case continuous long-read  
80 sequencing or PacBio CLR) that had been initially applied to the other ape references to  
81 minimize sequencing technology biases. This included sequence and assembly of primate  
82 genomes representing gibbon (*Nomascus leucogenys*), marmoset (*Callithrix jacchus*), and  
83 one owl monkey (*Aotus nancymaae*) (Table 1). Second, we wanted to leverage the higher  
84 accuracy and assembly contiguity of HiFi (high-fidelity) sequencing data by sequence and  
85 assembly of all NHP genomes where haplotypic differences could be distinguished. These  
86 served as a means to validate all fixed structural variation events as well as provide complete  
87 haplotype-resolved access to any particular regions of interest without the need to construct  
88 and annotate these different NHP genomes for yet a third time.

89

90

91 **RESULTS**

92 ***Genome assembly of NHP genomes***

93 Building on our previous analysis of African great ape genomes<sup>14,17,19</sup>, we first sequenced  
94 and assembled three additional female NHP genomes using CLR sequencing, namely, white-  
95 cheeked gibbon (*Nomascus leucogenys*), the common marmoset (*Callithrix jacchus*), and  
96 owl monkey (*Aotus nancymaae*). Each genome was sequenced to high depth (>56-fold  
97 coverage), assembled, and error corrected as described previously<sup>14,16,17,19</sup> (Supplementary  
98 Figure 1 and Supplementary Table 1). We generated highly contiguous (contig N50=9.9 to  
99 25 Mbp) squashed assemblies of ~2.84-2.9 Gbp with an overall sequence accuracy of  
100 >99.98% (Table 1 and Supplementary Table 1). Next, to further reduce sequencing error and  
101 increase our ability to investigate more complex regions, we sequenced the same eight NHP  
102 samples using PacBio HiFi sequencing<sup>17,27</sup> (Table 1; Supplementary Figure 2 and  
103 Supplementary Table 1). We used hifiasm to produce haplotype-resolved genomes that were  
104 substantially smaller among monkeys (5.84 to 6.23 Gbp, diploid) when compared to  
105 nonhuman apes<sup>21</sup> (6.12 to 6.98 Gbp). These HiFi assemblies are estimated to be more  
106 accurate (QV=42 to 58 or 99.9937% to 99.9998% accuracy) and significantly more  
107 contiguous (contig N50=19 to 104 Mbp) when compared to the CLR draft genome  
108 assemblies (Table 1 and Supplementary Figure 3).

109

110 ***NHP sequence divergence and incomplete lineage sorting (ILS)***

111 As a baseline for sequence divergence among the lineages, we mapped the HiFi sequence  
112 data from each NHP back to human and computed single-nucleotide divergence (Methods).  
113 The mean autosomal sequence divergence ranged from 1.3% to 9.83%, consistent with the  
114 expected phylogeny, and was predictably higher than that of the X chromosome (0.99% to  
115 8.24%; Figure 1a and 1b, Supplementary Table 2). We note that these estimates are also  
116 slightly higher than earlier reports likely because a great fraction of repetitive DNA is being  
117 included among NHPs<sup>8,19</sup>. For example, among the apes ~92% of the human genome is  
118 aligned in contrast to the New World monkey lineages where 64% and 59.7% of the  
119 sequence from owl monkey and marmoset are unambiguously aligned (Supplementary Table  
120 3). An assembly-based comparison yields similar results but involves a smaller fraction of  
121 the genome due to extensive and more complex forms of structural variation (Supplementary  
122 Figure 4 and Supplementary Table 3).

123

124 We used these data to generate a time-calibrated phylogeny for the nine primate species,  
125 including human (Figure 1a and 1b; Supplementary Tables 4-6). We constructed more than  
126 one million complete multiple sequence alignments (MSAs) at a resolution of 500 bp (518.9  
127 Mbp of aligned sequence). While the majority of trees (52.7%) are consistent with the  
128 generally accepted phylogeny, the fraction of alternate topologies is, once again, greater than  
129 previous estimates<sup>9,13,17,28</sup> (Figure 1c, Supplementary Table 4). Most of the difference can be  
130 attributed to potential ILS during African ape or great ape speciation as gene tree  
131 concordance factors show the lowest values in these two nodes (gene tree concordance=64.3  
132 and 62, respectively)<sup>29</sup>. Lineage-specific branch lengths are generally balanced with one  
133 notable exception: the owl monkey branch length is significantly shorter and divergence to  
134 human significantly lower when compared to marmoset (Figure 1a). An analysis of 16,244  
135 gene trees using human as an outgroup to both owl monkey and marmoset shows that the owl  
136 monkey evolves significantly slower ( $p=0$  autosome,  $p=6.85 \cdot 10^{-185}$  for the X chromosome)  
137 (Supplementary Figure 5). Excluding potential sites of ILS, we estimated split times of the  
138 species and find that mean split times of the apes better match the lower bounds of previous  
139 estimates<sup>30-36</sup> (Supplementary Table 7).

140

#### 141 ***Primate lineage-specific versus shared SVs***

142 We applied a three-pronged approach to discover and validate SVs ( $\geq 50$  bp) mapping to the  
143 euchromatic portion of the primate lineages<sup>37,38</sup>. Using read-based and assembly-based  
144 callers (pbsv, Sniffles and PAV), we first compared the eight NHP genomes against the  
145 human reference genome, including three additional human genomes (CHM13, HG00733  
146 and NA19240) to mitigate the effect of human polymorphism and missing variants in a  
147 particular reference (Supplementary Table 8). In total, we identified 2.23 million putative  
148 insertions and 1.89 million deletions in these nine lineages. Using both HiFi sequence data  
149 and genome assemblies, we validated 1.85 million insertions and 1.63 million deletions  
150 (mean validation rate: 86.79% and 89.37%, respectively) (Supplementary Table 9). We note  
151 that genome-based HiFi and CLR SV calling are highly congruent (>95%) although HiFi  
152 tended to recover larger insertions (Supplementary Figure 6). Finally, we generated Oxford  
153 Nanopore Technologies (ONT) data from the same primate DNA samples and manually  
154 inspected a subset (900 SV events) for confirmation using this orthogonal sequencing  
155 platform estimating a false positive rate and a false negative rate of ~2.6% and 11.4%,  
156 respectively (Supplementary Table 10).

157 To distinguish fixed from polymorphic events, we further genotyped (Methods) the validated  
158 SVs against Illumina whole-genome sequence (WGS) data from a panel of 120 genomes (30  
159 humans and 90 NHPs, Supplementary Table 11)<sup>39-43</sup>. We projected the 1,338,997 fixed  
160 events (441,453 deletions and 897,544 insertions) onto the primate phylogeny (Figure 2a;  
161 Supplementary Tables 12 and 13) classifying events as shared or lineage-specific<sup>17</sup>  
162 (Methods). The number of SV events correlates strongly with evolutionary genetic distances  
163 separating species (Figure 2b) with characteristic insertion peaks at ~6 kbp and 300 bp—full-  
164 length *L1* and *Alu* mobile element insertions (Supplementary Figure 7 and Supplementary  
165 Table 14). Remarkably, we estimate that 27.2% of the genome (819.47 Mbp) has been  
166 subjected to structural variation across these nine lineages with fixed insertions  
167 outnumbering deletions approximately two to one (the total length of shared and lineage-  
168 specific insertions is ~524.8 Mbp versus ~294.68 Mbp of deletions) (Figure 2a). The excess  
169 of insertions is greatest for the ancestral ape and African great ape lineages (~2- to 3-fold)  
170 (Figure 2a and Supplementary Table 13) and this twofold excess is still observed when  
171 calibrating for the number of fixed SNV differences<sup>44,45</sup> (Figure 2b; Supplementary Figures 8  
172 and 9).

173  
174 A small fraction of fixed primate SVs affect genes (~18.78 Mbp of deletions and ~1.31 Mbp  
175 insertions). Using human gene annotation as a guide, we annotated the fixed SVs against the  
176 human gene models (GRCh38, RefSeq) and the regulatory element database (ENCODE V3)  
177 with Variant Effect Predictor (VEP)<sup>46,47</sup>. These fixed SVs intersect 6,067 genes, including  
178 1,561 protein-coding genes, and 136,932 regulatory elements. The latter includes 2,389  
179 promoter-like (PLS) and 16,455 proximal enhancer-like signatures (pELS) potentially  
180 disrupted by 16,671 fixed SVs (Supplementary Table 15). We estimate that 244 genes and  
181 1,759 regulatory elements are novel and several are likely to confer functional effect  
182 (Supplementary Figures 10 and 11). Such is the case for the 3,741 bp *LIPA5* insertion shared  
183 in apes mapping to the last exon of the neuronal-function gene, astrotactin 2 (ASTN2), which  
184 encodes a glycoprotein that guides neuronal migration during the development of the central  
185 nervous system<sup>48,49</sup>. The insertion creates a novel transcript isoform resulting in a new exon  
186 in human (NM\_1884735) and this innovation is accompanied by a 1 base-pair deletion in this  
187 exon, which in gibbon, orangutan, and gorilla is incapable of read-through due to a  
188 frameshift from the reciprocal 1 bp insertion (Figure 2c and Supplementary Figure 12).  
189 Similarly, the Aggrecan (ACAN) gene, important in stature and brachydactyly in humans<sup>50</sup>,  
190 has been altered in the great ape lineage by a 60 bp deletion, which eliminates part of the

191 chondroitin sulfate attachment domain (Supplementary Figure 13). In gibbons, we identify a  
192 large ~42.7 kbp deletion of the neurogenesis-associated gene, trace-amine associated  
193 receptor 2, (*TAAR2*) along with seven of its enhancers (Figure 2d and Supplementary Figure  
194 14). Loss of this brain-expressed gene in knockout mice has been shown to result in higher  
195 levels of dopamine and lower levels of norepinephrine in the striatum and hippocampus  
196 respectively<sup>51</sup>. A complete list of these gene and gene-regulatory fixed SVs is provided along  
197 with additional discussion (e.g., *AR*, *SPATA1*, *ELN*, and *MAGEB16*) (Supplementary Tables  
198 16 and 17, Supplementary Figures 15-18, and Supplementary Discussion).

199

200 We also reassessed human-specific changes and the effect of potential reference biases in  
201 discovery. Importantly, 7,169 human-specific SVs have been reclassified, in part, because of  
202 the inclusion of more outgroup species in addition to the use of more accurate sequence  
203 aligner (minimap2 vs. blasr) that improves alignment within repetitive regions such as  
204 subtelomeres<sup>52,53</sup> (Supplementary Figures 19 and 20). Nevertheless, we identified 13  
205 additional genes and 252 additional regulatory elements as potentially disrupted compared to  
206 our previous report<sup>19</sup> (Supplementary Figures 21 and 22). This includes, for example, a 90-  
207 base pair deletion within the third exon of N-acetyltransferase 16 (*NAT16*) resulting in 30  
208 amino acid loss in human lineage with respect to all other NHPs. The event was confirmed in  
209 all humans by genotyping and by full-length transcript sequencing (Figure 2e and  
210 Supplementary Figure 23). *NAT16* is highly expressed in the brain and pituitary and is  
211 responsible for Nα-acetylhistidine synthesis, but its biological function remains unknown.

212

213 To assess the effect of using a human reference genome to classify such events, we repeated  
214 ape-specific SV analyses using an assembled African human genome and the orangutan ape,  
215 instead as the reference genomes to base the comparison. As expected, the analyses  
216 reclassified approximately 34 gene-disruption events and led to a reduction of SVs most  
217 notably with respect to insertions (Supplementary Figure 24). For example, using orangutan  
218 as a reference reduces the number of lineage-specific insertions in orangutan (56,389 vs.  
219 77,933), chimpanzee (2,020 vs. 4,471), bonobo (3,108 vs. 5,886), and human (13,446 vs.  
220 16,696) lineage-specific insertions (Supplementary Figures 25 and 26, Supplementary Table  
221 18). The intersect of these two sets provides the most conservative set of lineage-specific  
222 changes on each branch. Consistent with the previous analyses, we find that the number of  
223 insertions is ~2-3 times than that of deletions.

224

225 ***Structurally Divergent Regions (SDRs)***

226 In addition to increased accuracy and haplotype resolution, another major advantage of HiFi-  
227 based assemblies is their 4- to 6-fold increase in sequence contiguity (Table 1). During our  
228 comparison of monkey and ape chromosomes, we identified much larger, structurally  
229 divergent regions (SDRs) that had been missed or incompletely assayed by our standard SV  
230 analyses (Supplementary Figures 27 and 28). These regions were often gene-rich but had  
231 eluded complete characterization due to their sequence divergence and/or structural  
232 complexity<sup>54</sup>. We, therefore, developed a graph-based approach to more systematically  
233 identify such regions (>10 kbp in length) in apes and macaques that could not be readily  
234 mapped to the complete human genome (T2T-CHM13) with >85% sequence identity<sup>55</sup>. We  
235 identified 1,704 SDRs and validated 1,607 SDRs using two independent approaches<sup>56</sup>  
236 (validation rate: 94.3%; Methods) (Supplementary Tables 19 and 20). SDRs were large  
237 (average 127.4 kbp, Supplementary Figure 28) and enriched 3.6-fold for large segmental  
238 duplications (SDs) (Supplementary Figure 29; p=0). Specifically, 423 SDRs (26.3%) contain  
239 at least 10 kbp of annotated SDs while 1,184 appeared to map to relatively unique regions of  
240 the genome (Supplementary Tables 19 and 20), although subsequent sequence analysis  
241 identified 2.2% of these (1.07 Mbp) as lineage-specific SDs not present in human SD  
242 annotations.

243

244 Similar to the SVs, we genotyped all SDRs using Illumina WGS from primate population  
245 samples<sup>39-43</sup> and successfully assigned 1,050 of the SDRs to lineage-specific branches on the  
246 primate phylogeny (Supplementary Figure 30). However, 557 SDRs show evidence of  
247 recurrent or serial SVs among multiple NHP lineages and the majority (62.3% or 347/557)  
248 associate with SD sequences (Supplementary Table 19). We constructed a null model for the  
249 distribution of SDRs and identified 184 distinct hotspot regions where we predict significant  
250 large-scale and recurrent structural variation among different primate lineages (331 recurrent  
251 SDRs) (Figure 3a and Supplementary Table 21). Of these, 88% (162/184) harbor SDs and  
252 56% (103/184) of these hotspots correspond to 631 genes, including many known medically  
253 relevant regions such as *CFHR*, *RHD*, *LPA*, *APOL*, *AMY1* and the Major histocompatibility  
254 complex (MHC) locus (such as *MICA/MICB* and the complement *C4/C3* genes)<sup>57-60</sup> (Figure  
255 3a and Supplementary Figures 31-33). Others are completely novel or have been partially  
256 described based on analyses of specific primate genomes<sup>57-60</sup>. A gene ontology analysis  
257 predicts an expected enrichment for the known widespread loss of olfactory receptors in  
258 primates (p=3·10<sup>-85</sup>) but also genes associated with other biological processes, including

259 thiol-dependent ubiquitinyl hydrolase activity ( $p=1.9 \cdot 10^{-24}$ ), antimicrobial activity ( $p=2.2 \cdot 10^{-5}$ ), innate immune response ( $p=5 \cdot 10^{-5}$ ), neurotransmitter receptor activity ( $p=2.5 \cdot 10^{-4}$ ), etc. 260 (Supplementary Table 22). Notably, most of these enrichments are associated with core 261 duplicons including *DEFBs*, *NPIPs*, *RGPDs*, *CYPs*, *NBPFs*, *GOLGAs*, *UGTs*, *RHDs*, and 262 *USPs*<sup>60,61</sup> (Supplementary Table 23).

264

265 A few examples of these hotspot regions are illustrative. We confirmed, for example, that the 266 *CARD18* (caspase recruitment domain family member 18) was lost in the ancestral *Pan* 267 lineage by ~60 kbp deletion event<sup>7</sup>. We identified, however, a larger and independent 268 deletion of ~190 kbp in the gibbon lineage that completely removes the entire gene cluster— 269 *CARD16* (pLI=0.04), *CARD17* (pLI=0), and *CARD18* (pLI=0.05). A third independent 270 deletion of ~150 kbp removed yet another member, *CARD17*, in the owl monkey suggesting 271 that this entire gene family has been under relaxed selection during primate evolution (Figure 272 3b and Supplementary Figure 34). Other hotspots are more complex, such as the *OLAH-* 273 *ACBD7* region showing evidence of both gain and loss of genes (Figure 3c). In gorilla, 274 *OLAH* (pLI=0) is deleted by a ~32 kbp deletion (Supplementary Figure 35) whereas in 275 macaque the locus has been the target of ~190 kbp duplication that truncates *OLAH* in that 276 lineage but also creates a new copy of *ACBD7*, which is actively transcribed as a fusion gene 277 (Figure 3c). In *Pan*, the same region has been the target of a ~250 kbp SD that originated 278 from chromosome 12 and produces a *Pan*-specific transcript with an open-reading frame 279 (ORF) of 97 amino acids whose promoter region is hypomethylated (Figure 3d, 280 Supplementary Figure 36). This large insertion of an SD in the *Pan* lineage also had the 281 benefit of removing one of two directly orientated duplications flanking *MEIG* 282 (meiosis/spermiogenesis associated 1), theoretically eliminating recurrent 283 microdeletion/microduplication of *MEIG1* in the *Pan* lineage (Figure 3d and 3e). A 28 kbp 284 genomic duplication region has been depleted in orangutans, but this has not resulted in any 285 alteration of gene content (Supplementary Figure 37). *MEIG1* (pLI=0.05) is a 286 spermiogenesis-related gene and *MEIG1* deficiency severely disrupts mouse spermatogenesis 287 and is potentially associated in human infertility<sup>62-64</sup>.

288

289 In order to test the potential for SDRs to serve as cradles for gene innovation, we repeated 290 our SDR analysis in a more distantly related primate. Using our graph-based approach, we 291 compared human and marmoset and identified 697 SDRs (~38.45 Mbp) that could not be

292 orthologously aligned to the complete human reference genome. Next, we manually  
293 clustered them into 270 distinct SDR events since these two genomes are too divergent  
294 (Supplementary Table 24). For the purpose of gene discovery, we also generated ~5.13  
295 million full-length cDNA transcripts from 10 distinct primary tissues from the common  
296 marmoset (Table 1 and Supplementary Table 25). We identified five regions that showed  
297 evidence of novel or structurally divergent transcripts that lacked orthologous counterparts in  
298 the human genome (Supplementary Figure 38 and Supplementary Table 24). Of particular  
299 interest was a gene-rich region of human chromosome 13 that had been subject to a series of  
300 inversions and duplications increasing by ~350 kbp in size and adding nine putative  
301 marmoset-specific genes (Figure 4a). We searched for gene expression using the marmoset  
302 Iso-Seq transcript resource and confirmed expression for five of these—*VPS36*, *UTP14C*,  
303 *NEK5*, *THSD1*, and *CKAP2* broadly in the brain as well as other tissues (Figures 4b,  
304 Supplementary Figure 39 and Supplementary Table 26). In addition, our phylogenetic  
305 analysis estimates that the marmoset-specific duplication of the *THSD-NEK* region occurred  
306 ~11.9 million years ago (mya) and these duplicated genes maintain a protein-encoding ORF  
307 with numerous amino acid replacements as well as changes in gene structure when compared  
308 to progenitor copies (Supplementary Figure 40).

309

### 310 ***Recurrent RGPD duplications and restructuring of ape chromosome 2***

311 Our SDR analysis of apes identified five SDRs on human chromosome 2 associated with a  
312 single core dupilon: *RGPD* (chr2:105859737-114023252, p=0) (Figure 5a). Core duplions  
313 were previously described as actively transcribed gene families associated with the  
314 expansion of interspersed SDs in the human–ape lineage<sup>61</sup>. In particular, *RGPD* is a fusion  
315 gene/transcript formed by the duplication and juxtaposition of the two ancestral genes  
316 *RANBP2* and *GCC2* less than 15 mya<sup>65</sup>. Given the contiguity of the HiFi genome assemblies,  
317 we focused on a detailed reconstruction of the evolutionary history of this gene family across  
318 a ~7 Mbp region of chromosome 2 relating its expansion to large-scale structural changes  
319 and potential gene innovation associated with the SDRs in humans (Supplementary Figures  
320 41 and 42). No evidence of *RGPD* genes exist in macaques, marmosets, or owl monkeys  
321 where only the ancestral *RANBP2* and *GCC2* genes are found syntenically among all  
322 primates (Supplementary Figure 42). Phylogenetic analyses confirm its formation and  
323 general expansion in copy number in the ancestral ape lineage (Supplementary Figure 43).  
324 Both the phylogeny and the sites of integration, however, reveal that most interspersed  
325 duplications are independent—the result of recurrent SDs or gene conversion events (Figure

326 5a and 5b, Supplementary Figure 43). For example, none of the gibbon or orangutan  
327 duplicate copies map syntenically to each other or other African great apes—thus, although  
328 orangutan has multiple *RGPDs*, all originated independently and none have orthologs among  
329 the other apes and group as distinct clade within the tree (Figure 5b and Supplementary  
330 Figure 43). We identify only one paralogous gene, h*RGPD2*, that is syntenic and orthologous  
331 among the African great apes. Within the five different ape lineages, we estimate ~20  
332 independent mutation events (total length: ~1.2 Mbp) representing one of the most extreme  
333 examples of homoplasy (Figure 5a and Supplementary Figure 42).

334

335 Most of the *RGPD* interspersed SDs were accompanied by both local restructuring of the  
336 duplication blocks as well as larger scale structural rearrangements of the chromosome 2  
337 flanking sequence especially in association with large-scale inversions in different NHP  
338 lineages (Figure 5c and Supplementary Figure 44). Haplotype-resolved sequence assemblies  
339 allowed the origin and spread of lineage-specific copies to be distinguished phylogenetically  
340 (Figure 5b). Human *RGPD3* and *RGPD4* are not phylogenetically, for example, orthologs of  
341 chimpanzee *RGPD3* and *RGPD4* even though they appear syntenic (Figure 5b and  
342 Supplementary Figure 43) suggesting potential gene conversion. In addition, the emergence  
343 of many *RGPDs* in apes appears to have been driven by recurrent large-scale inversions,  
344 duplicative transpositions, and deletions within a ~7 Mbp genomic region over the last 15  
345 million years of evolution creating unique configurations and distinct copies in each ape  
346 lineage (Supplementary Figure 44).

347

348 *RGPD1* is a human-specific paralog predicted to have arisen ~570 thousand years ago (kya)  
349 within the *Homo* lineage at ~0.57 mya (Figure 5b). This specific copy has several amino acid  
350 replacements at the protein N-terminus with respect to all other human RGPDs—this change  
351 is predicted to alter the protein structure between h*RGPD1* and its antecedent h*RGPD2*<sup>66</sup>  
352 (Figure 5d). In this regard, it is interesting that the h*RGPD1* genomic region shows a dearth  
353 of genetic diversity based on the analysis of Human PanGenome Reference Consortium  
354 (HPRC) haplotype-resolved assemblies ( $\pi$  value= $4.65 \cdot 10^{-5}$ ,  $p < 0.05$ , TajimaD= -1.98)  
355 (Figure 5e and Supplementary Figure 45) consistent with the region potentially being  
356 subjected to a selective sweep specifically and recently in the human lineage.

357

358 In comparison to human, most of the copies mapping to bonobo and chimpanzee  
359 chromosome 2 represent independent expansions from ancestral *RANBP2* that also gave rise

360 to human *RGPD5*, *RGPD6*, and *RGPD8* (Supplementary Figure 43). Of note, *RGPD6* is a  
361 human-specific gene copy that arose via segmental duplication or gene conversion from  
362 human *RGPD5* most recently (~5.2 kya, 95% CI [0.002,16.08]) (Figure 5b). The interval  
363 between these human-specific copies, which includes *NPHP1*, is subjected to both inversion  
364 toggling and microdeletion associated with Joubert syndrome and juvenile nephronophthisis  
365 as a result of nonallelic homologous recombination (NAHR) between inverted and directly  
366 orientated duplications<sup>67-69</sup>, respectively (Figure 5f and Supplementary Figure 46). We  
367 examined 94 human phased haplotypes from the HPRC and Human Genome Structural  
368 Variation Consortium<sup>38,69-71</sup> and identified 11 distinct structural configurations—four  
369 predisposing to microdeletion (Figure 5g; Supplementary Figures 46-50 and Supplementary  
370 Table 27). We also identified a single pathogenic allele deleting *NPHP1* (HG00733) and  
371 confirmed maternal transmission (Supplementary Figures 51-53). A maximum likelihood  
372 phylogenetic analysis identified the most closely related (non-deleted) haplotype and  
373 breakpoint analysis confirms that the deleted allele arose from one of the haplotypes  
374 predisposing to microdeletion (Supplementary Figure 51). Given the recent evolutionary  
375 restructuring of this region of chromosome 2, it follows that this predisposition to  
376 microdeletion is specific to the human lineage.

377

## 378 **DISCUSSION**

379 Using three long-read sequencing platforms across multiple primate genera, we present a  
380 comprehensive analysis of SVs within euchromatic DNA of the primate order<sup>15,19</sup>. The use of  
381 HiFi data and inclusion of additional NHP species as well as genotyping in population  
382 samples significantly improves earlier surveys of fixed SV events<sup>39-43</sup> and extends the  
383 analysis deeper within the primate phylogeny. Among the great apes for example, we  
384 identify 13 genes and 1,759 regulatory elements not previously reported<sup>19</sup> (Supplementary  
385 Figures 21 and 22). The addition of other primate genomes identified lineage-specific SDR  
386 events in the gibbon (n=680), macaque (n=219), and marmoset (n=697) lineages  
387 (Supplementary Figure 30). Similarly, while we identify all 16 previously identified ape-  
388 specific genic SVs; 13/16 are no longer classified as (great) ape-specific SVs (Supplementary  
389 Table 28) due to the inclusion of other NHP lineages<sup>15</sup>. Finally, the use of a highly  
390 contiguous orangutan genome as an alternate reference, helped reduce earlier human genome  
391 reference biases by refining and polarizing the set of fixed SVs that occurred specifically  
392 since humans diverged from the other ape lineages (Supplementary Table 18). Among the  
393 6,067 genes (both coding and noncoding) and 136,932 regulatory DNA associated with fixed

394 SVs, we find a significant enrichment in transcription regulation ( $p=1.1 \cdot 10^{-9}$ ), sensory  
395 transduction ( $p=6.3 \cdot 10^{-3}$ ), cell division ( $p=2.3 \cdot 10^{-2}$ ), and vocal learning ( $3.4 \cdot 10^{-3}$ )  
396 (Supplementary Table 29). These data serve as a rich resource for the characterization of  
397 gene expression differences and candidate mutations for adaptation among NHPs.  
398

399 The overall topology of the primate phylogenetic tree is consistent with previous  
400 expectations with the proportion of ILS generally increasing as more of the repetitive content  
401 is accessed by long-read sequencing technology<sup>17</sup> (Figure 1). Our comparison of two New  
402 World monkeys lineages, however, reveals significant acceleration of the marmoset SNV  
403 branch length when compared to that of the owl monkey (branch length: 0.024 vs. 0.017).  
404 This finding is also consistent with the shorter blocks of synteny in the marmoset lineage  
405 when compared to the human genome (only 102 regions >500 kbp compared to 169 regions  
406 >500 kbp in the owl monkey) and the significant increase in the number of recent SDs (165.7  
407 Mbp in marmoset vs. 125.7 Mbp in owl monkey) (Supplementary Table 30). The slower  
408 evolution of the owl monkey lineage compared to marmoset may simply be a consequence of  
409 differences in reproductive longevity as has been proposed<sup>40</sup> or changes in the generation  
410 time of the two lineages during evolution. The three major clades of New World monkeys,  
411 however, are thought to have diverged over a short time frame (19-24 mya)<sup>35,36,72,73</sup> (Figure  
412 1a). Studying multi-generational pedigrees, Thomas and colleagues showed a 32.5%  
413 reduction in the rate of *de novo* mutation in owl monkey when compared to that of apes with  
414 an overall mutation rate of  $0.81 \cdot 10^{-8}$  per site per generation<sup>40</sup>. Our results suggest that this  
415 reduced mutation rate may be longstanding property of the *Aotinae* with the net consequence  
416 that the owl monkey genome is less derived when compared to marmoset. These findings  
417 have some practical considerations regarding the use of these different New World monkeys  
418 as models for human disease<sup>74-76</sup>.  
419

420 The greater accuracy afforded by HiFi sequencing allowed more complex regions of genetic  
421 variation to be assembled contiguously across the primates (e.g., MHC). We developed a  
422 graph-based approach to systematically identify 1,604 SDRs among apes and macaque  
423 (Figure 3) of which a third (n=557) showed evidence of recurrent structural variation and  
424 were enriched for SDs. We hypothesize that these hotspots of recurrent structural variation  
425 and their associated 631 genes (mean pLI=0.133) demarcate either regions of the ape genome  
426 no longer under selection (e.g., *CARD18*, *OLAH*, etc.) or regions where rapid structural

427 diversification has facilitated the emergence of new genes showing signatures of positive  
428 selection (e.g., *RGPD*, *NPIP*, *NPF*)<sup>77-79</sup> (Figure 5) and/or important for adaptive  
429 specializations in different primate lineages<sup>24,80,81</sup>. Ironically, the innovations often come at a  
430 cost with respect to fitness as the SDRs are associated with human disease susceptibility  
431 regions (e.g., 1q22.3, 2q13, 16p11.2, 10p13), such as the human-specific duplication of  
432 *RGPD5* and Joubert syndrome deletion alleles (Figure 5).

433

434 Our analysis also suggests that SDRs are common in the primate genome though with few  
435 exceptions these regions have not been considered as part of previous large-scale sequencing  
436 efforts because of 1) difficulties in their assembly and 2) challenges they pose in alignment  
437 even among closely related species when fully resolved. We identified, for example, SDRs in  
438 marmoset compared to owl monkey giving rise to marmoset-specific duplicate genes (Figure  
439 4). Using our resource of ~5.13 million full-length transcripts, we show that these duplicate  
440 genes are expressed in the brain, maintain an ORF, and emerged specifically since marmoset  
441 diverged from other owl monkey ~20 mya (Supplementary Figure 54). The ancestral genes  
442 have critical functions: *NEK5*, for example, is member of NimA family of serine/threonine  
443 protein kinases involved in cell differentiation while *CKAP2* (cytoskeleton associated protein  
444 2) is involved in cell division<sup>82,83</sup>. These findings caution against simply using human gene  
445 models to annotate NHP genomes or to assess NHP gene expression differences from single-  
446 cell RNA sequencing experiments. Understanding the gene innovations in such previously  
447 inaccessible complex regions of primate genomes will be critical to realizing the full  
448 potential of these species as models of human genetic disease<sup>74-76</sup>.

449

## 450 Materials and Methods

451 We sequenced and assembled eight NHP reference genomes using long-read PacBio HiFi  
452 and ONT sequencing chemistry and the hifiasm genome assembler<sup>21</sup>. All samples, with one  
453 exception, were female and correspond to the same samples used in previous studies as  
454 references, namely; Central chimpanzee (Clint)<sup>7</sup>, bonobo (Mhudiblu)<sup>17</sup>, Western gorilla  
455 (Kamilah)<sup>13</sup>, Sumatran orangutan (Susie)<sup>8</sup>, Northern white-cheeked gibbon (Asia)<sup>10</sup>, rhesus  
456 macaque (AG07107)<sup>16</sup>, common marmoset (CJ1700), and owl monkey (86718) (Table 1).  
457 We used pbsv, Sniffles, and PAV to characterize SVs and merged SVs using the SVPOP  
458 pipeline<sup>37,38</sup>. The merged calls were validated with HiFi sequencing data and assembly of  
459 select regions; ONT sequence data from the same specimens were used to calculate the false  
460 positive rate and validate assembly of select regions in our data set. The validated SVs were

461 genotyped by Paragraph using Illumina WGS data from 120 population samples<sup>16,39-43,84</sup>.  
462 VEP was used to annotate the functional disruption of SVs<sup>46</sup>. In addition to SVs (<20 kbp)  
463 identified by the three callers, we used a graph-based aligner (Mashmap) to identify large  
464 structural changes across apes and Old World monkey<sup>55</sup>, defined here as SDRs. SDR  
465 validation was based on haplotype-resolved assemblies and ONT data. The ONT data also  
466 were used to call methylation by Guppy<sup>85</sup>. We also generated full-length Iso-Seq data  
467 specifically from 10 diverse marmoset tissues and from a gibbon immortalized lymphoblast  
468 line. In the case of the marmoset, full-length RNA was prepared from 10 distinct tissues  
469 obtained upon necropsy from a different specimen (*Callithrix jacchus*). Genomic divergence  
470 analyses were based on HiFi sequencing data and genomes, respectively. Syntenic regions  
471 across New World monkey to apes and MSAs were constructed with minimap2 and  
472 mafft<sup>53,86</sup>. The phylogenetic analyses were performed using TREEeasy, IQTREE, and  
473 BEAST2<sup>87-89</sup>.

#### 474 **Acknowledgments**

475 We thank T. Brown for manuscript proofreading and editing. This article is subject to  
476 HHMI's Open Access to Publications policy. HHMI lab heads have previously granted a  
477 nonexclusive CC BY 4.0 license to the public and a sublicensable license to HHMI in their  
478 research articles. Pursuant to those licenses, the author-accepted manuscript of this article  
479 can be made freely available under a CC BY 4.0 license immediately upon publication.

480

#### 481 **Funding**

482 This work was supported, in part, by National Institutes of Health (NIH) grants HG002385,  
483 HG010169, and HG009081 to E.E.E.; GM147352 to G.A.L.; R01HG010485,  
484 U41HG010972 and U01HG010961 to B.P.; R01-AI-137011 and DP1-DA-046108 to S.L.S.;  
485 by Shanghai Pujiang Program (22PJ1407300) and Shanghai Jiao Tong University 2030  
486 Program (WH510363001-7) to Y.M.; by National Natural Science Foundation of China  
487 grants 82001372 to X.Y.; L.C. is supported by the P51 OD011092 (to the Oregon National  
488 Primate Research Center); E.E.E. is an investigator of the Howard Hughes Medical Institute.

489

#### 490 **Author contributions**

491 Y.M. and E.E.E. conceived the project; Y.M., W.T.H., K.M.M., K.H., A.P.L., P.A.A., A.R.,  
492 D.S.G., G.A.L., P.C.D., and E.E.E. generated sequencing data, assembled genomes, analyzed  
493 the data, and performed quality control analyses; X.Y., R.R., V.L.B., W.T.F., G.K.W., G.F.,

494 S.L.S., and W.C.W. contributed the marmoset and owl monkey samples; L.C. contributed the  
495 bonobo and gibbon samples; Y.M. performed the SNV divergence and ILS analyses; Y.M.,  
496 W.T.H., P.A.A., S.Z., G.A.L., H.J., and E.E.E. performed SV analyses; Y.M. performed  
497 SDR analyses; M.H., and B.P. generated gene model annotations; Y.M., D.P., and E.E.E.  
498 performed *NPHP1* haplotype analyses; Y.M., X.W., and Q.L. performed the protein structure  
499 prediction analyses. Y.M. and E.E.E. drafted the manuscript. All authors read and approved  
500 the manuscript.

501

## 502 Competing interests

503 E.E.E. is a scientific advisory board (SAB) member of Variant Bio, Inc. The other authors  
504 declare no competing interests.

505

## 506 Data and materials availability

507 The raw PacBio CLR, HiFi, and ONT data are deposited in NCBI under BioProject  
508 accession number PRJNA877605. The CLR and HiFi NHP assemblies are deposited in  
509 NCBI under BioProject accession numbers PRJNA941350- PRJNA941365. The marmoset  
510 Iso-Seq data are deposited under NCBI BioProject accession number PRJNA566173.

511

## 512 References

- 513 1 Watson, J. D. The human genome project: past, present, and future. *Science* 248, 44-  
514 49, (1990).
- 515 2 Lander, E. S. *et al.* Initial sequencing and analysis of the human genome. *Nature* 409,  
516 860-921, (2001).
- 517 3 Venter, J. C. *et al.* The sequence of the human genome. *Science* 291, 1304-1351  
518 (2001).
- 519 4 Gibbs, R. A. The Human Genome Project changed everything. *Nature reviews.*  
520 *Genetics* 21, 575-576, doi:10.1038/s41576-020-0275-3 (2020).
- 521 5 Nurk, S. *et al.* The complete sequence of a human genome. *Science* 376, 44-53  
522 (2022).
- 523 6 McConkey, E. H. *et al.* A primate genome project deserves high priority. *Science*  
524 289, 1295-1296 (2000).
- 525 7 Chimpanzee Sequencing Analysis Consortium. Initial sequence of the chimpanzee  
526 genome and comparison with the human genome. *Nature* 437, 69-87 (2005).
- 527 8 Locke, D. P. *et al.* Comparative and demographic analysis of orang-utan genomes.  
528 *Nature* 469, 529-533 (2011).
- 529 9 Prüfer, K. *et al.* The bonobo genome compared with the chimpanzee and human  
530 genomes. *Nature* 486, 527-531 (2012).
- 531 10 Carbone, L. *et al.* Gibbon genome and the fast karyotype evolution of small apes.  
532 *Nature* 513, 195-201, (2014).
- 533 11 Rogers, J. & Gibbs, R. A. Comparative primate genomics: emerging patterns of  
534 genome content and dynamics. *Nature Reviews Genetics* 15, 347-359 (2014).

- 535 12 Juan, D., Santpere, G., Kelley, J. L., Cornejo, O. E. & Marques-Bonet, T. Current  
536 advances in primate genomics: novel approaches for understanding evolution and  
537 disease. *Nature Reviews Genetics*, 1-18 (2023).
- 538 13 Scally, A. *et al.* Insights into hominid evolution from the gorilla genome sequence. *Nature* 483, 169-175 (2012).
- 539 14 Gordon, D. *et al.* Long-read sequence assembly of the gorilla genome. *Science* 352, aae0344 (2016).
- 540 15 He, Y. *et al.* Long-read assembly of the Chinese rhesus macaque genome and  
541 identification of ape-specific structural variants. *Nature communications* 10, 4233  
542 (2019).
- 543 16 Warren, W. C. *et al.* Sequence diversity analyses of an improved rhesus macaque  
544 genome enhance its biomedical utility. *Science* 370, eabc6617 (2020).
- 545 17 Mao, Y. *et al.* A high-quality bonobo genome refines the analysis of hominid  
546 evolution. *Nature* 594, 77-81 (2021).
- 547 18 Yang, C. *et al.* Evolutionary and biomedical insights from a marmoset diploid  
548 genome assembly. *Nature* 594, 227-233 (2021).
- 549 19 Kronenberg, Z. N. *et al.* High-resolution comparative analysis of great ape genomes.  
550 *Science* 360, eaar6343 (2018).
- 551 20 Logsdon, G. A., Vollger, M. R. & Eichler, E. E. Long-read human genome  
552 sequencing and its applications. *Nature Reviews Genetics* 21, 597-614 (2020).
- 553 21 Cheng, H., Concepcion, G. T., Feng, X., Zhang, H. & Li, H. Haplotype-resolved de  
554 novo assembly using phased assembly graphs with hifiasm. *Nature methods* 18, 170-  
555 175 (2021).
- 556 22 Rautiainen, M. *et al.* Telomere-to-telomere assembly of diploid chromosomes with  
557 Verkko. *Nature Biotechnology*, 1-9 (2023).
- 558 23 Mao, Y. & Zhang, G. A complete, telomere-to-telomere human genome sequence  
559 presents new opportunities for evolutionary genomics. *Nature methods* 19, 635-638  
560 (2022).
- 561 24 Dennis, M. Y. *et al.* Evolution of human-specific neural SRGAP2 genes by  
562 incomplete segmental duplication. *Cell* 149, 912-922 (2012).
- 563 25 Fiddes, I. T. *et al.* Human-specific NOTCH2NL genes affect notch signaling and  
564 cortical neurogenesis. *Cell* 173, 1356-1369. e1322 (2018).
- 565 26 Kawanishi, K. *et al.* Human species-specific loss of CMP-N-acetylneurameric acid  
566 hydroxylase enhances atherosclerosis via intrinsic and extrinsic mechanisms.  
567 *Proceedings of the National Academy of Sciences* 116, 16036-16045 (2019).
- 568 27 Logsdon, G. A. *et al.* The structure, function and evolution of a complete human  
569 chromosome 8. *Nature* 593, 101-107 (2021).
- 570 28 Mailund, T., Munch, K. & Schierup, M. H. Lineage sorting in apes. *Annual review of  
571 genetics* 48, 519-535 (2014).
- 572 29 Minh, B. Q., Hahn, M. W. & Lanfear, R. New methods to calculate concordance  
573 factors for phylogenomic datasets. *Molecular biology and evolution* 37, 2727-2733  
574 (2020).
- 575 30 Steiper, M. E. & Young, N. M. Primate molecular divergence dates. *Mol Phylogenetic  
576 Evol* 41, 384-394, (2006).
- 577 31 Wilkinson, R. D. *et al.* Dating primate divergences through an integrated analysis of  
578 palaeontological and molecular data. *Systematic biology* 60, 16-31, (2011).
- 579 32 Prado-Martinez, J. *et al.* Great ape genetic diversity and population history. *Nature*  
580 499, 471-475, (2013).
- 581 33 Pozzi, L. *et al.* Primate phylogenetic relationships and divergence dates inferred from  
582 complete mitochondrial genomes. *Mol Phylogenetic Evol* 75, 165-183, (2014).

- 585 34 de Manuel, M. *et al.* Chimpanzee genomic diversity reveals ancient admixture with  
586 bonobos. *Science* 354, 477-481, (2016).
- 587 35 Vanderpool, D. *et al.* Primate phylogenomics uncovers multiple rapid radiations and  
588 ancient interspecific introgression. *PLoS biology* 18, e3000954, (2020).
- 589 36 Álvarez-Carretero, S. *et al.* A species-level timeline of mammal evolution integrating  
590 phylogenomic data. *Nature* 602, 263-267, (2022).
- 591 37 Sedlazeck, F. J. *et al.* Accurate detection of complex structural variations using  
592 single-molecule sequencing. *Nature methods* 15, 461-468 (2018).
- 593 38 Ebert, P. *et al.* Haplotype-resolved diverse human genomes and integrated analysis of  
594 structural variation. *Science* 372, eabf7117 (2021).
- 595 39 Prado-Martinez, J. *et al.* Great ape genetic diversity and population history. *Nature*  
596 499, 471-475 (2013).
- 597 40 Thomas, G. W. *et al.* Reproductive longevity predicts mutation rates in primates.  
598 *Current Biology* 28, 3193-3197. e3195 (2018).
- 599 41 Rogers, J. *et al.* The comparative genomics and complex population history of Papio  
600 baboons. *Science Advances* 5, eaau6947 (2019).
- 601 42 Okhovat, M. *et al.* Co-option of the lineage-specific LAVA retrotransposon in the  
602 gibbon genome. *Proceedings of the National Academy of Sciences* 117, 19328-19338  
603 (2020).
- 604 43 Byrska-Bishop, M. *et al.* High-coverage whole-genome sequencing of the expanded  
605 1000 Genomes Project cohort including 602 trios. *Cell* 185, 3426-3440. e3419  
606 (2022).
- 607 44 Marques-Bonet, T. *et al.* A burst of segmental duplications in the genome of the  
608 African great ape ancestor. *Nature* 457, 877-881 (2009).
- 609 45 Sudmant, P. H. *et al.* Evolution and diversity of copy number variation in the great  
610 ape lineage. *Genome research* 23, 1373-1382 (2013).
- 611 46 McLaren, W. *et al.* The ensembl variant effect predictor. *Genome biology* 17, 1-14  
612 (2016).
- 613 47 Moore, J. E. *et al.* Expanded encyclopaedias of DNA elements in the human and  
614 mouse genomes. *Nature* 583, 699-710 (2020).
- 615 48 Behesti, H. *et al.* ASTN2 modulates synaptic strength by trafficking and degradation  
616 of surface proteins. *Proceedings of the National Academy of Sciences* 115, E9717-  
617 E9726 (2018).
- 618 49 Bauleo, A. *et al.* Rare copy number variants in ASTN2 gene in patients with  
619 neurodevelopmental disorders. *Psychiatric Genetics* 31, 239-245 (2021).
- 620 50 Sentchordi-Montané, L. *et al.* Heterozygous aggrecan variants are associated with  
621 short stature and brachydactyly: description of 16 probands and a review of the  
622 literature. *Clinical endocrinology* 88, 820-829 (2018).
- 623 51 Efimova, E. V. *et al.* Trace amine-associated receptor 2 is expressed in the limbic  
624 brain areas and is involved in dopamine regulation and adult neurogenesis. *Frontiers  
625 in Behavioral Neuroscience* 16 (2022).
- 626 52 Chaisson, M. J. & Tesler, G. Mapping single molecule sequencing reads using basic  
627 local alignment with successive refinement (BLASR): application and theory. *BMC  
628 bioinformatics* 13, 1-18 (2012).
- 629 53 Li, H. Minimap2: pairwise alignment for nucleotide sequences. *Bioinformatics* 34,  
630 3094-3100 (2018).
- 631 54 Porubsky, D. *et al.* Gaps and complex structurally variant loci in phased genome  
632 assemblies. *bioRxiv*, (2022).

- 633 55 Jain, C., Koren, S., Dilthey, A., Phillippy, A. M. & Aluru, S. A fast adaptive  
634 algorithm for computing whole-genome homology maps. *Bioinformatics* 34, i748-  
635 i756 (2018).
- 636 56 Yang, X. *et al.* A refined characterization of large-scale genomic differences in the  
637 first complete human genome. *bioRxiv*, (2022).
- 638 57 Sekar, A. *et al.* Schizophrenia risk from complex variation of complement component  
639 4. *Nature* 530, 177-183 (2016).
- 640 58 Cantsilieris, S. *et al.* Recurrent structural variation, clustered sites of selection, and  
641 disease risk for the complement factor H (CFH) gene family. *Proceedings of the  
642 National Academy of Sciences* 115, E4433-E4442 (2018).
- 643 59 Thamadilok, S. *et al.* Human and nonhuman primate lineage-specific footprints in the  
644 salivary proteome. *Molecular biology and evolution* 37, 395-405 (2020).
- 645 60 Vollger, M. R. *et al.* Segmental duplications and their variation in a complete human  
646 genome. *Science* 376, eabj6965 (2022).
- 647 61 Jiang, Z. *et al.* Ancestral reconstruction of segmental duplications reveals punctuated  
648 cores of human genome evolution. *Nature genetics* 39, 1361-1368 (2007).
- 649 62 Khan, N. *et al.* Crystal structure of human PACRG in complex with MEIG1 reveals  
650 roles in axoneme formation and tubulin binding. *Structure* 29, 572-586. e576 (2021).
- 651 63 Zhang, Z. *et al.* MEIG1 is essential for spermiogenesis in mice. *Proceedings of the  
652 National Academy of Sciences* 106, 17055-17060 (2009).
- 653 64 Du, R. *et al.* Efficient typing of copy number variations in a segmental duplication-  
654 mediated rearrangement hotspot using multiplex competitive amplification. *Journal  
655 of human genetics* 57, 545-551 (2012).
- 656 65 Ciccarelli, F. D. *et al.* Complex genomic rearrangements lead to novel primate gene  
657 function. *Genome research* 15, 343-351 (2005).
- 658 66 Jumper, J. *et al.* Highly accurate protein structure prediction with AlphaFold. *Nature*  
659 596, 583-589 (2021).
- 660 67 Parisi, M. A. *et al.* The NPHP1 gene deletion associated with juvenile  
661 nephronophthisis is present in a subset of individuals with Joubert syndrome.  
662 *American journal of human genetics* 75, 82-91, (2004).
- 663 68 Gana, S., Serpieri, V. & Valente, E. M. Genotype-phenotype correlates in Joubert  
664 syndrome: A review. *Am J Med Genet C Semin Med Genet* 190, 72-88, (2022).
- 665 69 Porubsky, D. *et al.* Recurrent inversion polymorphisms in humans associate with  
666 genetic instability and genomic disorders. *Cell* 185, 1986-2005. e1926 (2022).
- 667 70 Liao, W.-W. *et al.* A draft human pangenome reference. *bioRxiv*, 2022.2007.  
668 2009.499321 (2022).
- 669 71 Wang, T. *et al.* The Human Pangenome Project: a global resource to map genomic  
670 diversity. *Nature* 604, 437-446 (2022).
- 671 72 Schneider, H. The current status of the New World monkey phylogeny. *Anais da  
672 Academia Brasileira de Ciências* 72, 165-172 (2000).
- 673 73 Perelman, P. *et al.* A molecular phylogeny of living primates. *PLoS genetics* 7,  
674 e1001342 (2011).
- 675 74 Baer, J. F., Weller, R. E. & Kakoma, I. *Aotus: the owl monkey*. (Academic Press,  
676 2012).
- 677 75 Okano, H., Hikishima, K., Iriki, A. & Sasaki, E. in *Seminars in fetal and neonatal  
678 medicine*. 336-340 (Seminars in fetal and neonatal medicine).
- 679 76 Grillner, S. *et al.* Worldwide initiatives to advance brain research. *Nature  
680 neuroscience* 19, 1118-1122 (2016).
- 681 77 Nuttle, X. *et al.* Emergence of a Homo sapiens-specific gene family and chromosome  
682 16p11.2 CNV susceptibility. *Nature* 536, 205-209 (2016).

- 683 78 Hsieh, P. *et al.* Evidence for opposing selective forces operating on human-specific  
684 duplicated TCAF genes in neanderthals and humans. *Nature communications* 12,  
685 5118 (2021).
- 686 79 Hsieh, P. *et al.* Adaptive archaic introgression of copy number variants and the  
687 discovery of previously unknown human genes. *Science* 366, eaax2083 (2019).
- 688 80 Ju, X.-C. *et al.* The hominoid-specific gene TBC1D3 promotes generation of basal  
689 neural progenitors and induces cortical folding in mice. *Elife* 5, e18197 (2016).
- 690 81 Dennis, M. Y. *et al.* The evolution and population diversity of human-specific  
691 segmental duplications. *Nature ecology & evolution* 1, 0069 (2017).
- 692 82 Prosser, S. L., Sahota, N. K., Pelletier, L., Morrison, C. G. & Fry, A. M. Nek5  
693 promotes centrosome integrity in interphase and loss of centrosome cohesion in  
694 mitosis. *Journal of Cell Biology* 209, 339-348 (2015).
- 695 83 McAlear, T. S. & Bechstedt, S. The mitotic spindle protein CKAP2 potently  
696 increases formation and stability of microtubules. *Elife* 11, e72202 (2022).
- 697 84 Chen, S. *et al.* Paragraph: a graph-based structural variant genotyper for short-read  
698 sequence data. *Genome biology* 20, 1-13 (2019).
- 699 85 Liu, Y. *et al.* DNA methylation-calling tools for Oxford Nanopore sequencing: a  
700 survey and human epigenome-wide evaluation. *Genome biology* 22, 1-33 (2021).
- 701 86 Katoh, K. & Standley, D. M. MAFFT multiple sequence alignment software version  
702 7: improvements in performance and usability. *Molecular biology and evolution* 30,  
703 772-780 (2013).
- 704 87 Bouckaert, R. *et al.* BEAST 2: a software platform for Bayesian evolutionary  
705 analysis. *PLoS computational biology* 10, e1003537 (2014).
- 706 88 Nguyen, L.-T., Schmidt, H. A., Von Haeseler, A. & Minh, B. Q. IQ-TREE: a fast and  
707 effective stochastic algorithm for estimating maximum-likelihood phylogenies.  
708 *Molecular biology and evolution* 32, 268-274 (2015).
- 709 89 Mao, Y., Hou, S., Shi, J. & Economou, E. P. TREEEasy: An automated workflow to  
710 infer gene trees, species trees, and phylogenetic networks from multilocus data. *Mol  
711 Ecol Resour* 20, (2020).
- 712

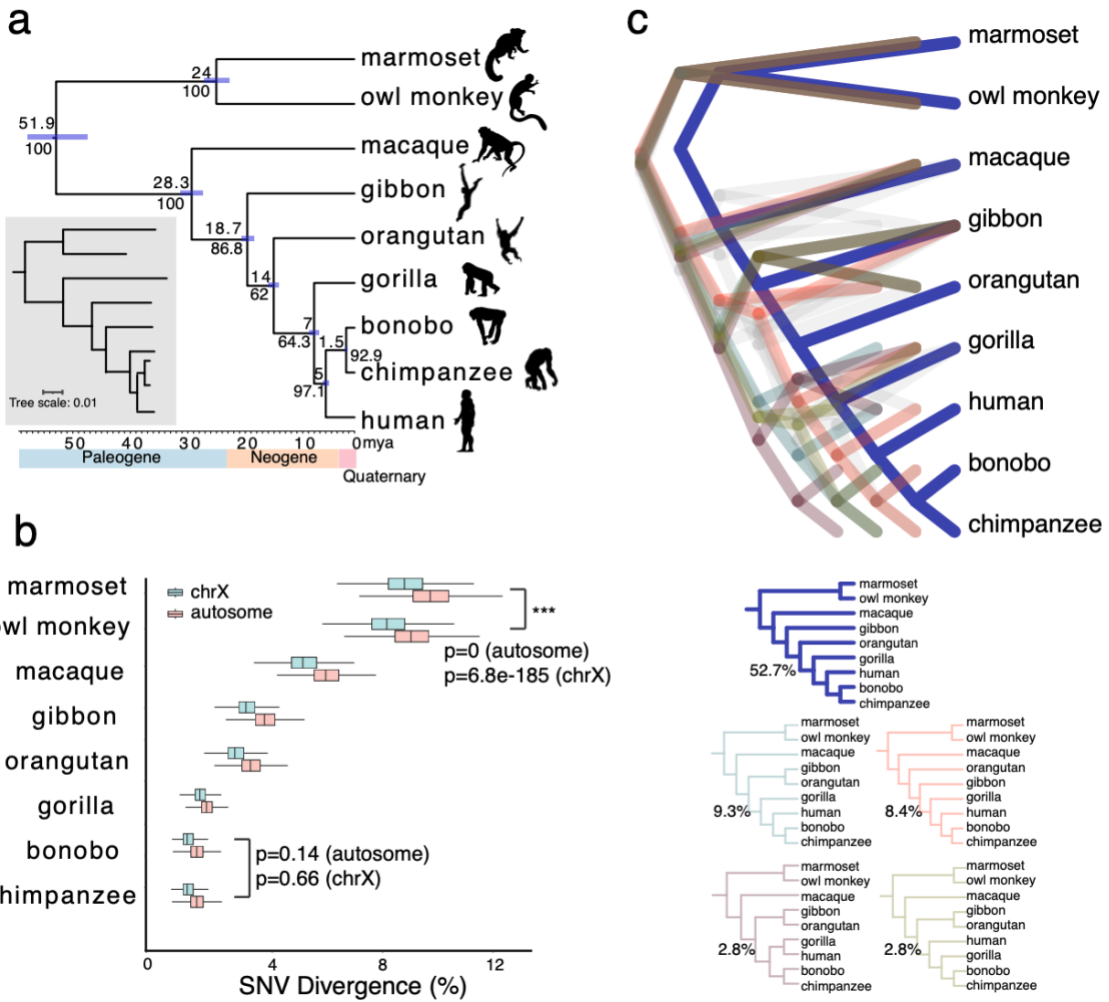
713 **Table 1. Primate genome sequence and assembly**

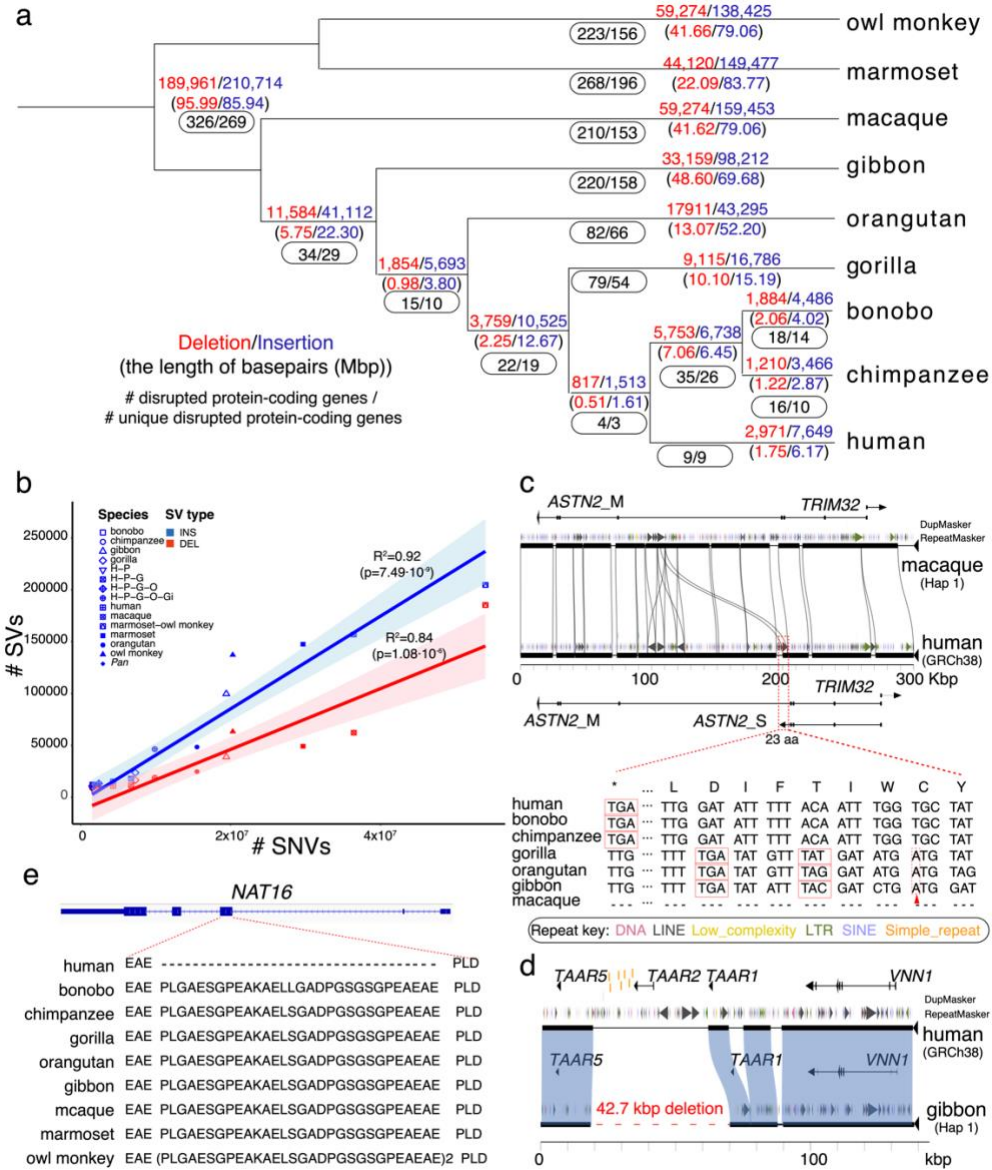
714

Common name	Scientific name	Individual ID	S e x	CLR raw data and assembly			HiFi raw data and assembly			Iso- Seq (Gbp)	ONT (Gbp)
				reads (coverage)	assembly (contig N50, Mbp)	QV	reads (coverage)	assembly (contig N50, Mbp)	QV hap1/ hap2		
Chimpanzee	<i>Pan troglodytes</i> (common chimpanzee)	Clint_PTR	M	117	12.27	39.19	37	66.89 /49.98*	45/44	1.94	294 (178*)
Bonobo	<i>Pan paniscus</i> (pygmy chimpanzee)	Mhudiblu_PP_A	F	74	15.06	39.25	39	50.45 /36.22*	47/47	1.38	124*
Gorilla	<i>Gorilla gorilla gorilla</i> (western lowland gorilla)	Kamilah_GGO	F	84.3	9.52	38.72	31	38.19 /37.87*	46/46	1.84	264*
Orangutan	<i>Pongo abelii</i> (Sumatran orangutan)	Susie_PAB	F	94.9	11.07	34.83	43	62.38/ 58.39*	42/42	1.09	272 (126*)
Gibbon	<i>Nomascus leucogenys</i> (northern white-cheeked gibbon)	Asia_NLE	F	92.5*	12.78*	38.65	31*	44.67 /34.99*	43/43	15.25 *	97*
Macaque	<i>Macaca mulatta</i> (Rhesus monkey)	AG07107_M_MU	F	66	46.61	36.18	29	18.81 /19.01*	51/52	104.5 8	329 (231*)
Marmoset	<i>Callithrix jacchus</i> (white-tufted-ear marmoset)	CJ1700_CJA	F	66*	25.23*	42.95 *	39*	103.97 /87.06*	58/58	18.43 *	NA
Owl monkey	<i>Aotus nancymaae</i>	86718_ANA	F	56.3*	9.85*	37.4*	31*	55.92 /44.99*	57/57	NA	91*

715 \* New data in this study

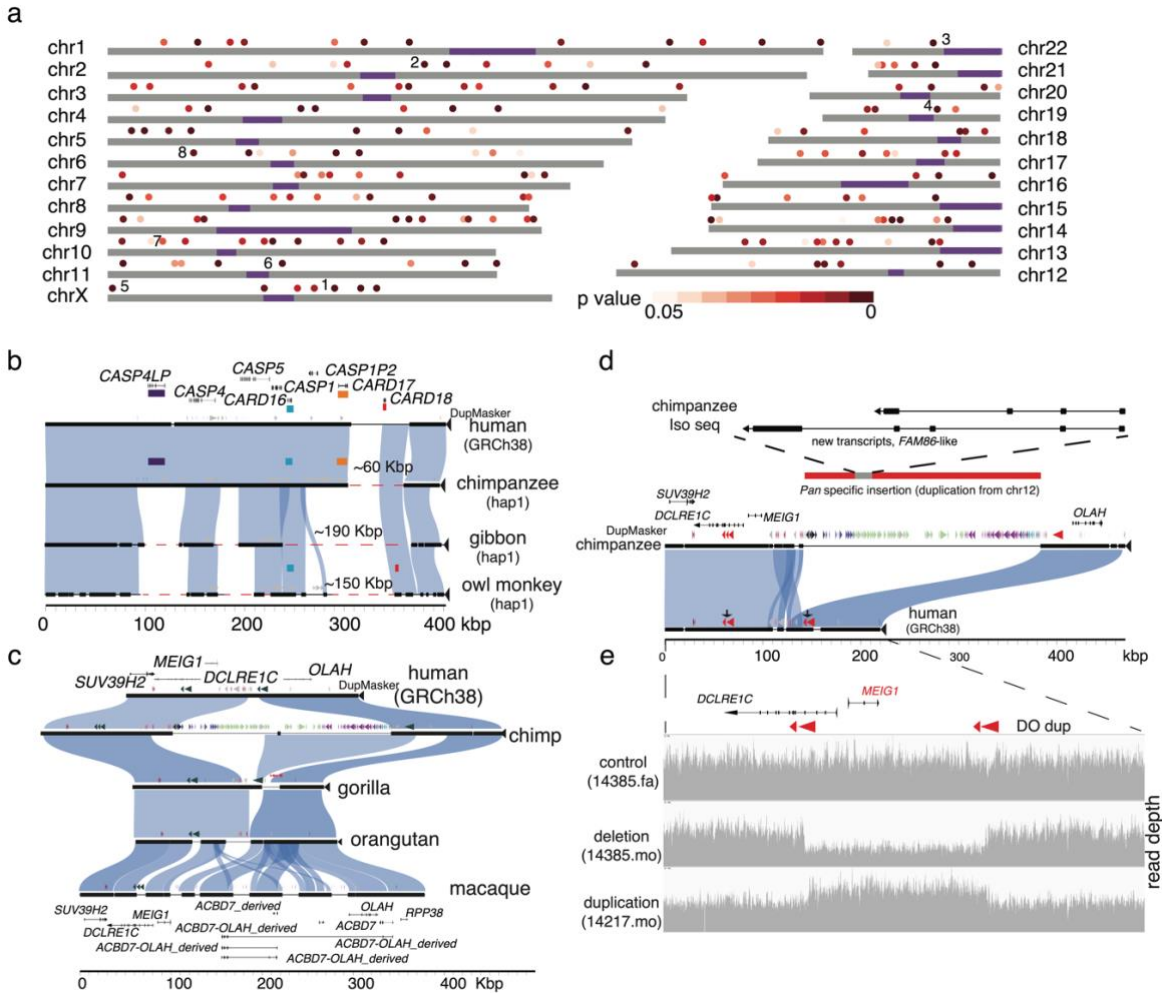
716 **Figures**





735

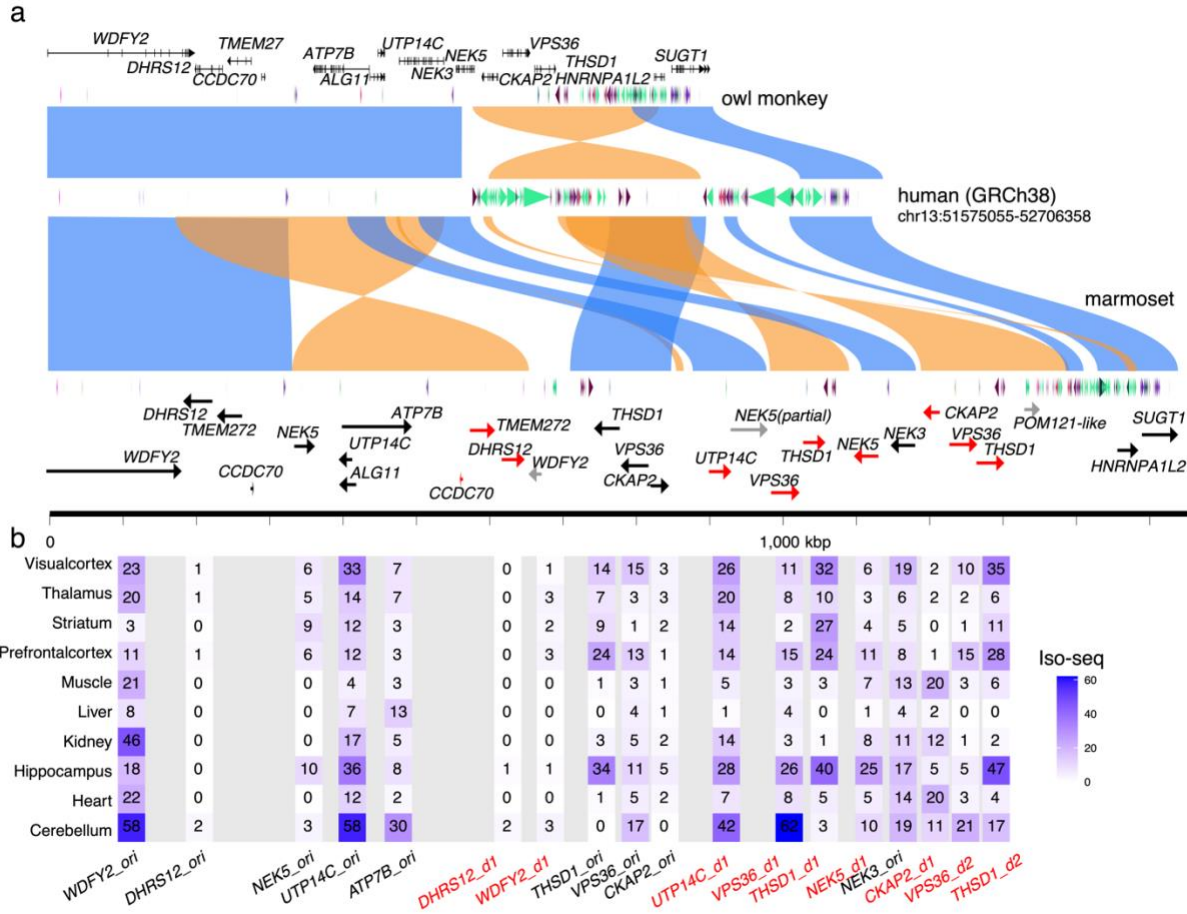
736 **Figure 2. Primate genome structural variation.** (a) The number of fixed structural variants  
737 (SVs) including deletions (red) and insertions (blue) are shown for each branch of the  
738 primate tree (number of events above the line and number of Mbp below). The number of  
739 “disrupted” protein-coding genes based on human RefSeq models are also indicated (black  
740 oval) with the total number of events (first number) and the subset specific to each lineage  
741 (second number). (b) The number of fixed SVs correlates with the accumulation of SNVs in  
742 each lineage (comparison to GRCh38) for both deletions (red) and insertions (blue). (c) An  
743 ape-specific fixed *L1* insertion (shown with a red dashed line box) in the human genome but  
744 not in the macaque genome (Miropeats alignment) serves as an exapted exon of the short  
745 isoform of astrotactin 2, *ASTN2*, in human. The coding sequences of the exon are shown in  
746 the bottom panel. The red triangles represent 1 bp insertion resulting in a frameshift in  
747 gorilla, orangutan, and gibbon. The red box represents the stop codon. (d) A 42.7 kbp  
748 lineage-specific deletion in the gibbon genome (red dashed line) deletes *TAAR2* and seven  
749 enhancers (shown in orange) compared to the human (GRCh38) (Miropeats comparison).  
750 (e) A 90 bp deletion (30 amino acids) human-specific deletion of *NAT16* (NM\_001369694)  
751 removes 30 amino acids in humans compared to all other NHPs.



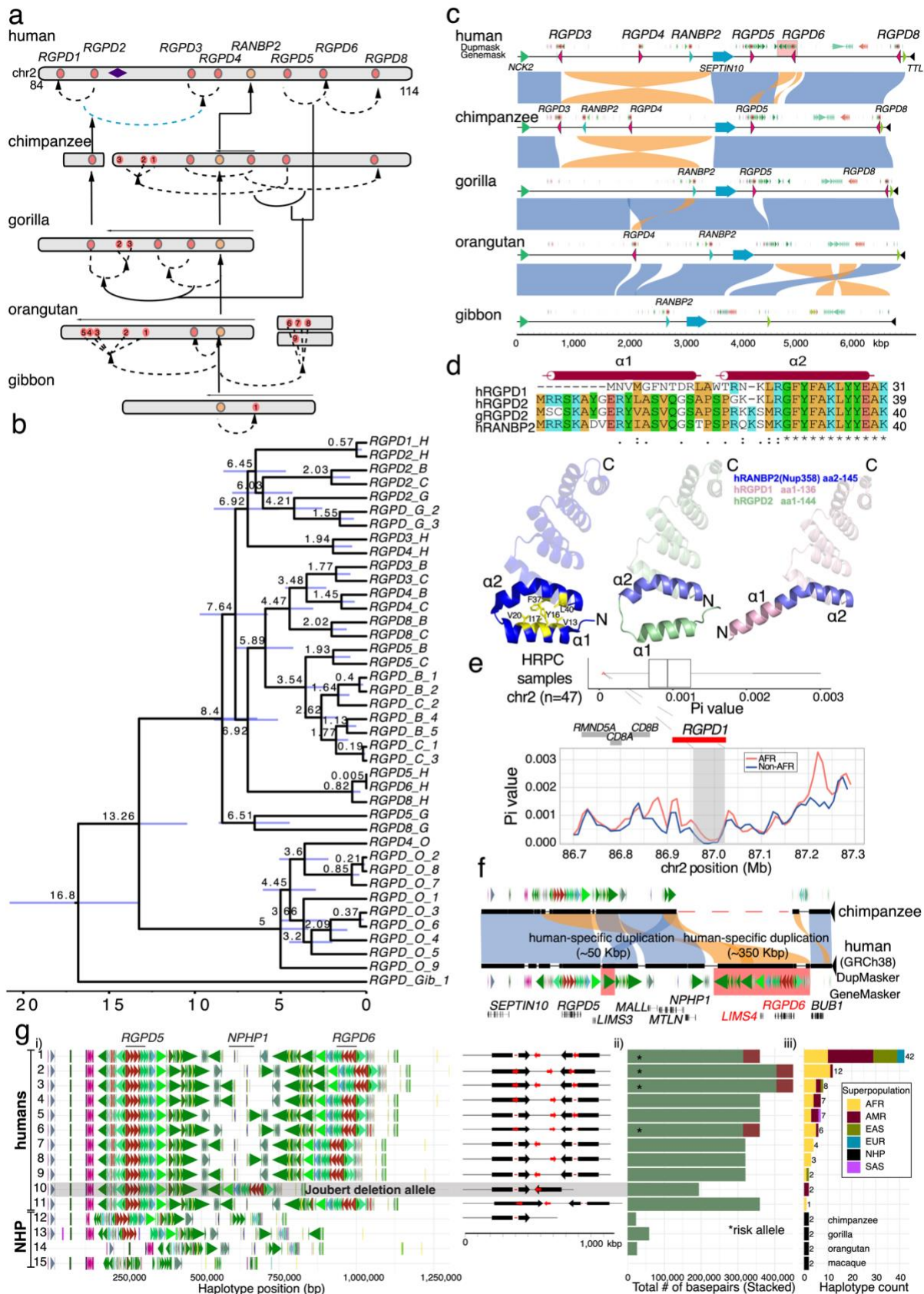
752

753 **Figure 3. Structurally divergent regions (SDRs) of the primate genome. (a)** A schematic  
754 of human chromosomes (T2T-CHM13) depicts SDR hotspots where recurrent  
755 rearrangements occur in excess. Heat map indicates significance based on simulation model  
756 (dark ( $p=0$ ) to light red ( $p=0.05$ )). Centromeres are depicted in purple. Enumerated regions  
757 identify specific gene families or regions of biomedical interest (1: *UPRT*, 2: *RGPDs*, 3:  
758 *USP41*, 4: *ZNFs*, 5. *IL3RA\_2*, 6: *CARDs*, 7: *OLAH*, and 8: *MHC*). **(b)** Recurrent deletion of  
759 the caspase recruitment domain (*CARD*) gene family. SafFire plot  
760 (<https://github.com/mrvollger/SafFire>) shows a ~58 kbp deletion of *CARD18* (orange) in the  
761 *Pan* lineage, multiple deletions (~190 kbp total) in gibbon of *CARD16* (blue), *CARD17* (red)  
762 and *CARD18*, and multiple deletions ~150 kbp, including *CARD17* (red), in marmoset.  
763 **(c)** SafFire plot of SDR mapping to genes *OLAH*, *MEIG1*, and *ABCD7* in human shows a  
764 large ~250 kbp insertion of segmental duplications (SDs; colored arrowheads) in chimpanzee  
765 within the intergenic region between *MEIG1* and *OLAH*. *OLAH* is deleted in gorilla by an  
766 independent lineage-specific deletion (~30 kbp). Multiple independent insertion events in  
767 macaque add ~190 kbp of sequence, including a duplication of *OLAH* in macaque. Full-  
768 length transcript sequencing of macaque using Iso-Seq supports the formation of five novel  
769 transcripts, including four *OLAH-ABCD* fusion events and a derived *ABCD7* (macaque gene  
770 models below). **(d)** The chimpanzee-specific 250 kbp SD from chromosome 12 creates a  
771 novel multi-exonic gene model supported by Iso-Seq transcript sequencing in chimpanzee  
772 (upper panel) with an unmethylated promoter (Supplementary Figure 36). The insertion

773 simultaneously deletes one of two directly orientated (DO) SDs in chimpanzee. (e) In  
 774 humans, the DO repeats associate with the breakpoints of recurrent deletions and  
 775 duplications of the spermiogenesis gene *MEIG1*. Two females carrying a deletion and a  
 776 duplication (as measured by sequence read depth) are depicted from a population sample of  
 777 19,584 genomes (CCDG, <https://ccdg.rutgers.edu/>). The carrier frequencies for microdeletion  
 778 and microduplication in control samples are 0.026% and 0.189%, respectively.  
 779



780  
 781 **Figure 4. Marmoset-specific genes in a SDR.** (a) Saffire plot comparing the organization  
 782 of a gene-rich region of ~1.1 Mbp in human (middle), owl monkey (top), and marmoset  
 783 (bottom) genomes. Human and marmoset differ mainly by a large 250 kbp inversion (orange)  
 784 associated with the addition of 150 kbp of SD at the boundary of the inversion in humans  
 785 (colored arrowheads). The corresponding region in marmoset has expanded by ~400 kbp due  
 786 to inversion and marmoset-specific SDs creating marmoset-specific paralogs (red arrows) of  
 787 *CCDC70*, *TMEM272*, *DHRS12*, *UTP14C*, *ATP7B*, *VPS36*, *NEK5* and *CKAP2*. (b) Iso-Seq  
 788 full-length non-chimeric transcript sequencing from 10 marmoset primary tissues confirms  
 789 transcription of 8/10 of the paralogous copies and the maintenance of an open-reading frame  
 790 in at least six of these marmoset-specific gene candidates.  
 791



792

793

794

795

**Figure 5. Evolution, selection, and disease susceptibility of the *RGPD* gene family**

(a) Schematic depicting *RGPD* genes (red dots) compared to its progenitor gene *RANBP2*

(a) Schematic depicting *RNF43* genes (red dots), compared to its progenitor gene *RNF43L* (orange dot) in human, chimpanzee, gorilla, orangutan, and gibbon. Shared ancestral copies

796 among the lineages are indicated (vertical arrows) in contrast to lineage-specific duplications  
797 (black) or gene conversion events (blue dashed arced arrow). The majority of copies have  
798 expanded in a lineage-specific fashion in each ape lineage. **(b)** A maximum likelihood tree  
799 based on a 58.98 kbp MSA of 40 *RGPD* great ape copies outgrouped with a sole gibbon  
800 copy. Nodes are dated with BEAST2 with the mean age of divergence shown above the node  
801 (95% CI blue bar) for human (H), bonobo (B), chimpanzee (C), gorilla (G), orangutan (O),  
802 and gibbon (Gib) copies. The analysis confirms lineage-specific expansion with all nodes  
803 receiving 100% posterior possibility. **(c)** A comparison of ~7 Mbp on chromosome 2 among  
804 ape genomes showing that large breakpoints in synteny (colored rectangles) often correspond  
805 to sites of *RGPD* SD insertions (blue arrows). **(d)** Human genetic diversity (pi) calculated in  
806 20 kbp windows (slide 10 kbp) from 94 haplotype-resolved human genomes (HPRC) for a  
807 700 kbp region of chromosome 2. A segment mapping to the human-specific gene *RGPD1*  
808 shows the lowest genetic diversity on chromosome 2 (top panel, red arrow) in haplotypes of  
809 both African (red) and non-African (blue) descent. The data suggest that the *RGPD1* region  
810 may have been under recent selection in the ancestral human population. **(e)** AlphaFold  
811 predictions of the protein N-terminus structure RANBP2 (blue), h*RGPD1* (pink), and  
812 h*RGPD2* (green) predict that differences in amino acid composition alter the secondary  
813 structure of two alpha helices ( $\alpha$ 1 and  $\alpha$ 2) in the human-specific *RGPD1* copy. The X-ray  
814 crystal protein structure of hRANBP2 (Nup358, PDB: 4GA0) confirms that the  $\alpha$ 1 and  $\alpha$ 2  
815 interface is maintained as a result of critical hydrophobic amino acids located in the N-  
816 terminus. Specific amino acid changes in h*RGPD1* break the hydrophobic interface between  
817  $\alpha$ 1 and  $\alpha$ 2 but not in the ancestral h*RGPD2* or RANBP2 predicting the emergence of a  
818 human-specific protein structure. **(f)** Saffire plot (top panel) comparing the chimpanzee  
819 genome and human highlights the formation of a 350 kbp human-specific duplication  
820 creating *RGPD6* (red shading). **(g)** Analysis of 94 human haplotypes shows that the *RGPD6*  
821 locus is largely fixed among all humans but that the organization of the flanking SDs differs  
822 significantly. We identify 11 distinct structural haplotypes in the human population  
823 predicting both disease susceptibility as well as protective haplotypes for nonallelic  
824 homologous recombination (NAHR). NAHR between inverted repeats (large black arrows)  
825 predisposes to recurrent inversion of the region while NAHR between directly orientated  
826 repeats (red arrows) deletes the *NPHP1* allele creating the pathogenic allele associated with  
827 juvenile nephronophthisis and milder forms of Joubert syndrome<sup>67</sup>. This predisposition to  
828 disease, thus, arose as a result of the emergence of human-specific duplication of the *RGPD*  
829 gene family.  
830